Determination of the melting point depression of PB-1-CO_2 solutions through image analysis

Lucía Doyle
lucia.doyle@hcu-hamburg.de HafenCity University, Hamburg

Abstract
In the context of replacing polyurethane foam in DH pre-insulated pipes due to the toxicity of the diisocyanates, and facilitating recycling by eliminating the need to separate material layers of the sandwich structure, the foaming of PB-1 with CO_2 is being studied. The assessment of the plasticization effect induced by CO_2 in the polymer melt and determination of the melting point depression is required for the establishment and optimization of the foaming processing window. In this paper, a method for the determination of the melting point through image analysis is presented, validated and used for the study of PB-1 – CO_2 solutions. The obtained results through image analysis agree with those obtained with differential scanning calorimetry, validating the method. The CO_2 - induced melting point depression of PB-1 was determined as $\Delta T = 14°C$.

Introduction

Heating accounted for 50% of the global energy consumption in 2018, being so the largest energy end-use (IEA, 2019). The integration of renewable energy and waste heat sources could be largely facilitated by District Heating and Cooling (DHC). The backbone of DHC is the piping network, which enables the distribution and exchange of heat and cold between different producers and consumers. The use of polyurethane (PU) pre-insulated pipes has been a fundamental element for the transition from the 2nd to the 3rd Generation DHC (Lund et al., 2014). The PU acts both as insulation, ensuring and significantly increasing the energy efficiency of the system, and as bond between the heat medium pipe and the casing. The toxicity of the diisocyanates (ZAPP, 1957) required for the PU manufacturing and the recently approved restriction on their use (European Commission, 2020) challenge the continuity of PU pre-insulated pipes. With this background, the team of Technical Infrastructure Management HCU opened a research line on alternative polymeric foams which could replace PU in DHC pipelines in 2019 (Doyle, 2021; Doyle & Weidlich, 2019; Doyle & Weidlich, 2020; Doyle & Weidlich, 2021). This includes both the evaluation of commercial foams for the application as well as the foaming of other polymers. With the final goal of developing a pre-insulated pipe made out of a single material, as to facilitate recycling by eliminating the problematic of layer separation in sandwich constructions, the foaming of semicrystalline polybutene-1 (PB-1) is being studied. As for blowing agents, inert gases, mainly CO_2, are considered for environmental reasons.

The success of the foaming process and the morphology of resulting foams is strongly related to the foaming temperature. The foaming temperature window is found between the melting temperature (Tm) and the glass transition temperature (Tg) in the case of amorphous polymers, and between Tm and the crystallization temperature (Tc) for the case of semicrystalline polymers (Di Maio & Kiran, 2018; Sarver et al., 2018). The obtained expansion ratio and cell morphology are conditioned by the relative distance of the foaming temperature from the melting and crystallization temperatures of the polymer-CO_2 dissolution under equilibrium (Sarver et al., 2018). It is well known that the dissolution of CO_2 in a polymer matrix can cause a plasticization effect (Pasquali, Comi, Pucciarelli, & Bettini, 2008; Reignier, Gendron, & Champagne, 2007; Sarver et al., 2018; Takahashi, Hassler, & Kiran, 2012) resulting in a depression of Tm, Tg and Tc, causing a shift on the processing window. Energy savings also arise from the possibility to process at lower temperatures (Frerich, 2015). The determination of these temperatures under CO_2 environment is of great importance for the correct setting and optimization of the process parameters.

ISBN: 978-3-947972-33-3
DOI: 10.34712/142.26

Different techniques have been used for the determination of the melting point depression of polymer – CO_2 mixes. Reignier et al. (2007) used high pressure differential scanning calorimetry (HP-DSC) with Poly-ε-Caprolactone (PLC) and CO_2. Kelly et al (2013) used infrared spectroscopy in a high pressure cell with PLC and CO_2. Takebayashi et al. (2014) used near infrared spectroscopy (NIR) with a high-pressure cell for biphenyl and naphthalene under high-pressure CO_2. Frerich (2015) studied the melting behavior of PLA, PBS and PLA-PHS and CO_2 with a scanning transitiometer in a high-pressure cell. Lian et al. (2006) measured the carbon dioxide-induced melting point depression of PCL and PBS though the light transmission change through a view cell. A lamp was placed on one end of the view cell and images captured on the other end via a borescope attached to a videocamera. The polymer chip was placed in the optical path blocking the light, the melting was observed by the sudden light transmission through the cell. It could not be derived if the change detection was human based or computer based. Analogously, Takahashi et al. (2012) studied the melting behavior of biodegradable polyesters in CO_2 at high pressures through changes in the light intensity through the polymer with a view cell, using a photodetector for measuring the light intensity change. Pasquali et al. (2008) studied the meting point reduction of PEG 1500 in supercritical CO_2 via photographs through a view cell. The temperature was fixed and pressure increased until the polymer melting onset, defined as the appearance of the first liquid drop. However, it is not specified how the first drop is detected.

Aside from common the high-pressure cell, the presented methods require complex equipment or rely on human decision to detect a change on a set of images. However, human-scored image analysis is qualitative (Carpenter et al., 2006), and may be exposed to subjectivity and bias, leading to non-reproductible results. Therefore, automated image analysis is preferred. In this paper, a method for the determination of the melting point of polymer CO_2 mixes through digital image analysis and processing is presented and used for the characterization of Polybutene-1 – CO_2 solutions. Tests were undertaken in an autoclave with sapphire windows which allowed for image acquisition.

Data on the melting point depression of PB-1 CO_2 binary system has not been found available in the open literature. Its determination provides valuable information for the optimization of the foaming temperature.

Methods

As materials, PB-1 kindly provided by LyondellBasell, and CO_2 of >99.8% purity purchased from Westfalen were used.

Melting experiments were conducted in an autoclave having two windows opposite each other (Eurotechnica GmbH, Bargteheide, Germany). The autoclave is heated with a heat jacket and CO_2 is injected with a piston pump. The autoclave's inner environment is monitored with a temperature sensor type K with a precision of ±1 °C and a digital pressure sensor with a precision of 0,5%. A light source with variable intensity is placed by one of the windows and a camera (Fastcam SA-X2, Photron Limited, Japan) on the opposite window. The trigger of the camera is coupled to the autoclave control system, so that pressure and temperature are logged simultaneously to the image acquisition. A sketch of the system is provided in Fig.1

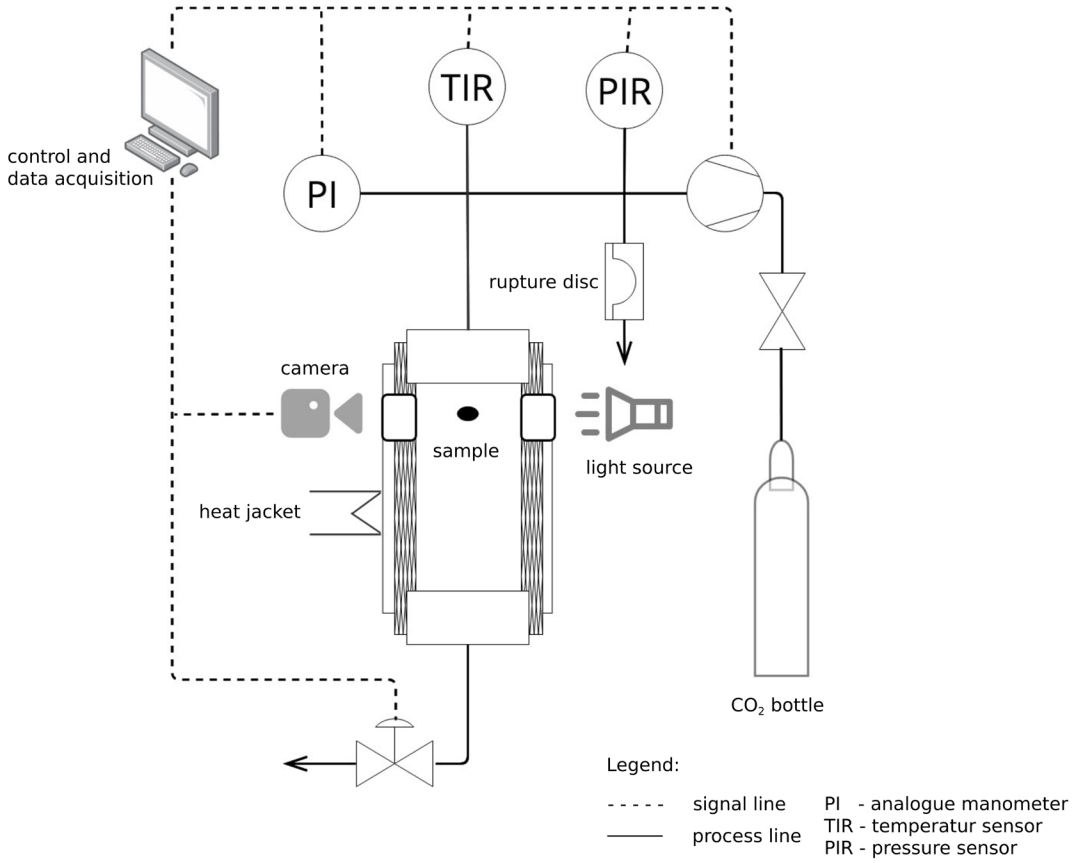

Fig. 1: Schematic representation of the autoclave with coupled image acquisition system

After reaching the required temperature, a pellet is placed centred in the optical path, on an optical glass support. The autoclave is purged 3 times with CO_2 before each trial. CO_2 is then introduced with a stepwise increase in pressure. Images are acquired in 20 s intervals and data logged accordingly. Trials were conducted in triplicate.

An image processing and analysis pipeline was developed using the open-source software Cell Profiler (Carpenter et al., 2006; Kamentsky et al., 2011) version 4.1.3. The main steps included converting each image to greyscale, inverting image intensities, identifying the pellet (segmentation) and measuring the pellet. The full list of parameters measured is presented in Table 1. The pipeline is available at *https://github.com/LuciaDoyle/MeltingPoint_ImageAnalyis.git*

Area	Eccentricity	Median Radius
Bounding Box Area	Equivalent Diameter	Min Feret Diameter
Bounding Box Maximum X	Euler Number	Minor Axis Length
Bounding Box Maximum Y	Extent	Orientation
Bounding Box Minimum X	Form Factor	Perimeter
Bounding Box Minimum Y	Major Axis Length	Solidity
Center X	Max Feret Diameter	Center X
Center Y	Maximum Radius	Center Y
Compactness	Mean Radius	Center Z

Tab. 1: Parameters measured for the pellet in each image

Reproducibility was evaluated by running multiple sets of experiments and comparing the results. The method was validated through comparing the results of melting under atmospheric conditions obtained from the image analysis with the typical differential scanning calorimetry (DSC) curve provided by the manufacturer. For the tests under pressure, the duration of the intervals was established after running successive trials with increasing interval duration to confirm the attainment of equilibrium conditions.

Once the method was validated, the melting point depression of PB-1 was determined by executing successive runs at different temperatures. In each run the temperature would be fixed, and CO_2 pressure increased in 5 bar steps. Reported results were executed with an initial stabilization time of 2 h at the first pressure level and the successive pressure increases conducted in 1 h intervals.

Results

Method Validation

In order to validate the method, the relationship between geometrical deformation measured through the image analysis and polymer melting was proven. For this, a pellet was placed in the view cell and progressively heated up to 150 °C, which is above the melting point of PB-1, reported in the data sheet as 131°C.

The obtained sequence of image measurements is compared with the typical PB-1 DSC curve provided by the manufacturer in Fig. 2. For ease of analysis, eccentricity and major axis length were selected as reference parameters. Eccentricity is defined as the ratio of the distance between the foci of the ellipse and its major axis length, corresponding e=0 to a circle. Major axis length is length of the major axis of the ellipse that has the same normalized second central moments as the region, given in pixels (Rocha, Velho, & Carvalho, 2002).

It should be noted that PB-1 is polymorphic and undergoes crystal–crystal transformation at room temperature. When cooling from the melt, it crystallizes into Form II, which is metastable and characterized by a tetragonal unit cell. It then undergoes transformation into Form I stable crystals (Boor & Mitchell, 1963; Jones, 1963; Natta, Corradini, & Bassi, 1960), a process reported to have a duration of around 10 days depending on the storage conditions (Hadinata et al., 2007). Data reported corresponds to the melting of Form I.

Figure 2. (a) presents the parameters eccentricity and major axis length measured through the images (b) the DSC heating ramp, (c) the first image of the sequence, corresponding to the pellet in the solid state and (d) the last image of the sequence, corresponding to the pellet in the molten state.

A very good correlation between graphs (a) and (b) can be observed, showing how the selected geometrical parameters correlate unequivocally with the melting event. Fig.2 (c) shows the first image of the sequence, and (d) the last, where the change in geometry can be observed. The change is not abrupt enough as to determine the onset with ease through the naked eye. It can be observed that the major axis length decreases during the melting event, which seams counterintuitive. It should be noted that when the region is fitted to an ellipse, it does not necessarily have its major axis parallel to the x axis. Moreover, since the best fit ellipse is found per image, it may change its orientation between images. Indeed it does change orientation during the melting event, causing the effect of the major axis length decreasing.

For the determination of the melting point of the polymer-CO_2 solution, the selected procedure was to fix a temperature and progressively increase the pressure, which was conducted in 5 bar steps, given the constant volume of the autoclave. The melting point depression is explained in terms of solubility effect, with the CO_2 acting as diluent in the melt (Lian et al., 2006). In order to ensure equilibrium conditions, care was taken in establishing the pressure increase duration steps. Trials were conducted with increasingly longer time steps, from 30 minutes to 2 hours. Procedure was fixed at 1 h time steps after a 2 h stabilization period at the initial conditions.

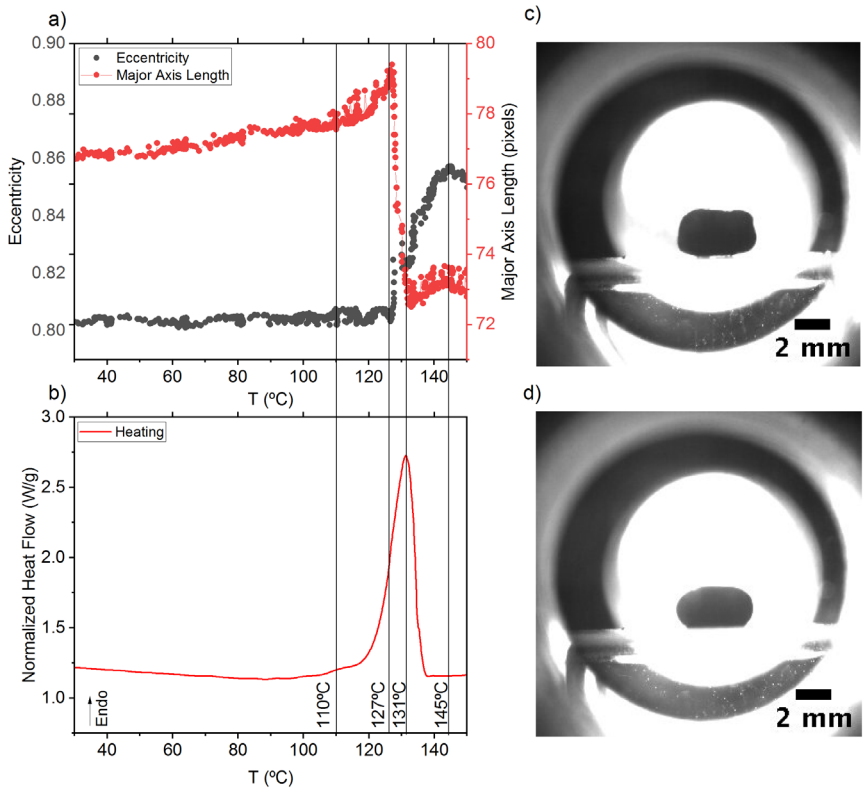

Fig. 2: (a) pellet deformation measured from the images during temperature increase. (b) DSC heating ramp. (c) initial pellet image. (d) last pellet image (molten)

Determination of melting point depression of PB-1 under CO_2

Representative runs for different set temperature are presented in Fig. 3. Additional trials at 112ºC and 105ºC was executed, were no melting was achieved with the pressures run up to 110 bar. The arrows highlight the melting point.

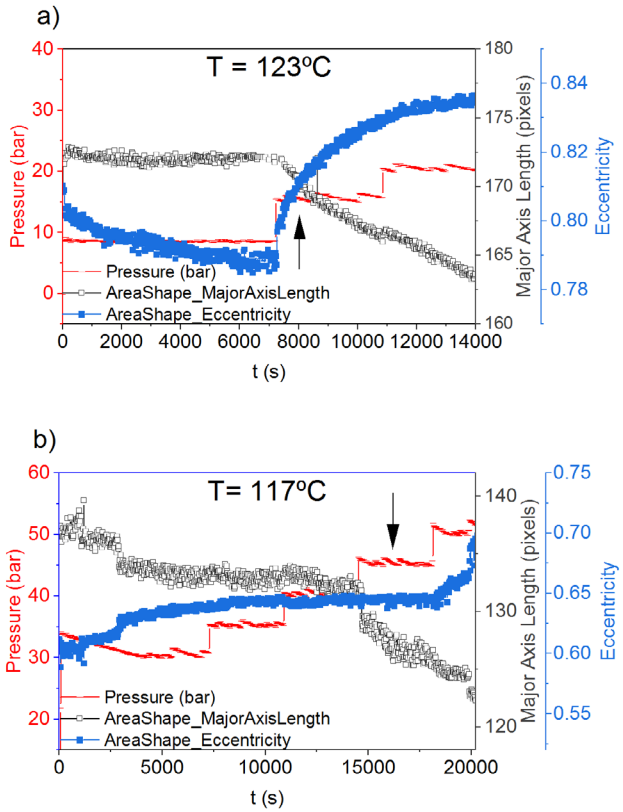

Fig. 3: Representative runs conducted at T = 123ºC (a) and 117ºC (b)

The obtained melting points as a function of pressure are given in Fig. 4. As can be seen, the melting point of PB-1 decreases linearly down to 117°C, with a pressure of 45 bar. This represents a ΔTm depression of 14°C.

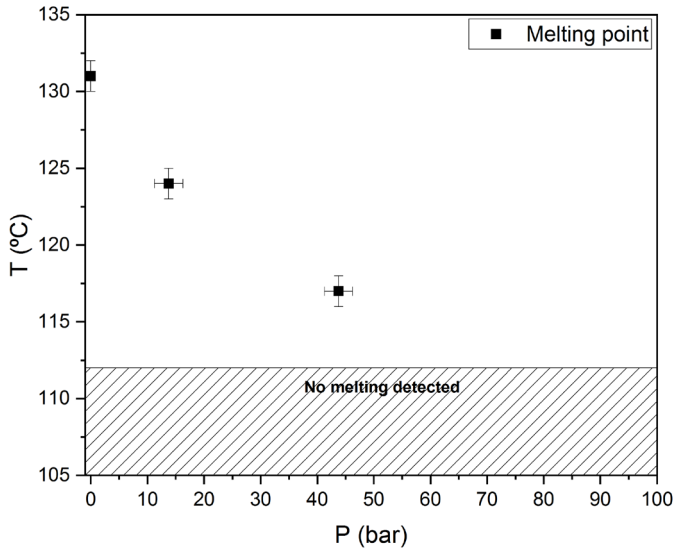

Fig. 4: Melting point of PB-1 in the presence of CO_2 at different pressures

The shape of the plot corresponds to that typically encountered in other polymer-CO_2 solutions, where the melting point decreases linearly with P until an abrupt change in slope occurs, from which the melting point remains more or less costant (Lian et al., 2006; Pasquali et al., 2008; Sarver et al., 2018; Takahashi et al., 2012). This changes in behaviour are explained through solubility effects at low pressures, as the addition of low concentrations of a diluent in a melt depresses the pure component melting point, and by hydrostatic pressure effect increasing the melting temperature at higher pressures (Swaan Arons & Diepen, 1963). In order to measure the values after the kink point, a variable cell would be required, as to fix a temperature and progressibly increase the pressure. The extent of the melting point depression can be correlated to the amount of absorbed CO_2 (Fukné-Kokot, König, Knez, & Škerget, 2000; Pasquali et al., 2008; Sarver et al., 2018), which is dependent on the applied pressure at a given temperature.

The CO_2 – induced plastitization effect observed in PB-1 is consistent with that reported by (Shi, Wu, Li, Liu, & Zhao, 2009) through the reduction of Tc. In their study, they report a depression of Tc from 90°C under atmosferic conditions to 60°C under supercritical CO_2 at 8 MPa when free cooling from the melt at 170°C, as detected with in-situ FTIR. This data also complements our findings towards the establishment of the processing window, since Tc cannot be detected through the here presented method. It should be however noted that unlike Tm, Tc is a second order transition and its value dependent on the cooling rate applied during the measurement (van Krevelen & Nijenhuis, 2009). The cooling rate at which the “free-cooling” occurred in the experiments by (Shi et al., 2009) is not reported. Data from the manufacturer provides a Tc of 71°C at a rate of 10°C/min, suggesting a much slower rate in the study by Shi et al.

Conclusion

This work demonstrates that the measurement of a sample’s geometrical features through image analysis is a powerful technique for the determination of the melting point in polymers and polymer-CO_2 solutions.

The melting point depression of PB-1-CO_2 mixtures was observed and quantified to ΔT=14°C. This provides useful information for the study and optimization of PB-1 foaming with CO_2.

Acknowledgement

The author would like to thank Werner Rothhöft (Lyondellbasell) for providing the PB-1 and Marcus Illguth (HCU) for programming the autoclave control software and Easter Egg hunt.

Literature

Boor, J., & Mitchell, J. C. (1963). Kinetics of crystallization and a crystal-crystal transition in poly-1-butene. Journal of Polymer Science Part A: General Papers, 1(1), 59–84.

Carpenter, A. E., Jones, T. R., Lamprecht, M. R., Clarke, C., Kang, I. H., Friman, O., et al. (2006). CellProfiler: image analysis software for identifying and quantifying cell phenotypes. Genome biology, 7(10), R100.

Di Maio, E., & Kiran, E. (2018). Foaming of polymers with supercritical fluids and perspectives on the current knowledge gaps and challenges. The Journal of Supercritical Fluids, 134, 157–166.

Doyle, L., & Weidlich, I. (2019). Mechanical Behaviour of Polylactic Acid Foam as Insulation Under Increasing Temperature. Environmental and Climate Technologies, 23(3), 202–210.

Doyle, L., & Weidlich, I. (2020). Recyclable Insulating Foams for High Temperature Applications. In Proceedings of The First International Conference on Green Polymer Materials 2020 (p. 7200).

Doyle, L. (2021). Extrusion foaming behavior of polybutene-1. Toward single-material multifunctional sandwich structures. Journal of Applied Polymer Science, 15, 51816.

Doyle, L., & Weidlich, I. (2021). Sustainable insulation for sustainable DHC. Energy Reports, 7, 150–157.

European Commission (2020). Commission Regulation (EU) 2020/1149 of 3 August 2020 amending Annex XVII to Regulation (EC) No 1907/2006 of the European Parliament and of the Council concerning the Registration, Evaluation, Authorisation and Restriction of Chemicals (REACH) as regards diisocyanates: (EU) 2020/1149. In Official Journal of the European Union.

Frerich, S. C. (2015). Biopolymer foaming with supercritical CO2—Thermodynamics, foaming behaviour and mechanical characteristics. The Journal of Supercritical Fluids, 96, 349–358.

Fukné-Kokot, K., König, A., Knez, Ž., & Škerget, M. (2000). Comparison of different methods for determination of the S–L–G equilibrium curve of a solid component in the presence of a compressed gas. Fluid Phase Equilibria, 173(2), 297–310.

Hadinata, C., Boos, D., Gabriel, C., Wassner, E., Rüllmann, M., Kao, N., & Laun, M. (2007). Elongation-induced crystallization of a high molecular weight isotactic polybutene-1 melt compared to shear-induced crystallization. Journal of Rheology, 51(2), 195–215.

IEA (2019). Renewables 2019. IEA. Retrieved October 29, 2021, from https://www.iea.org/reports/renewables-2019.

Jones, A. T. (1963). Polybutene-1 – type II crystalline form. Journal of Polymer Science Part B: Polymer Letters, 1(8), 455–456.

Kamentsky, L., Jones, T. R., Fraser, A., Bray, M.-A., Logan, D. J., Madden, K. L., et al. (2011). Improved structure, function and compatibility for CellProfiler: modular high-throughput image analysis software. Bioinformatics (Oxford, England), 27(8), 1179–1180.

Kelly, C. A., Harrison, K. L., Leeke, G. A., & Jenkins, M. J. (2013). Detection of melting point depression and crystallization of polycaprolactone (PCL) in scCO2 by infrared spectroscopy. Polymer Journal, 45(2), 188–192.

Lian, Z., Epstein, S. A., Blenk, C. W., & Shine, A. D. (2006). Carbon dioxide-induced melting point depression of biodegradable semicrystalline polymers. The Journal of Supercritical Fluids, 39(1), 107–117.

Lund, H., Werner, S., Wiltshire, R., Svendsen, S., Thorsen, J. E., Hvelplund, F., & Mathiesen, B. V. (2014). 4th Generation District Heating (4GDH). Energy, 68, 1–11.
Natta, G., Corradini, P., & Bassi, I. W. (1960). Crystal structure of isotactic poly-alpha-butene. Il Nuovo Cimento, 15(S1), 52–67.

Pasquali, I., Comi, L., Pucciarelli, F., & Bettini, R. (2008). Swelling, melting point reduction and solubility of PEG 1500 in supercritical CO2. International journal of pharmaceutics, 356(1-2), 76–81.

Reignier, J., Gendron, R., & Champagne, M. F. (2007). Autoclave Foaming of Poly(ε-Caprolactone) Using Carbon Dioxide: Impact of Crystallization on Cell Structure. Journal of Cellular Plastics, 43(6), 459–489.

Rocha, L., Velho, L., & Carvalho, P. (2002). Image moments-based structuring and tracking of objects. In L. M. G. Gonçalves & S. R. Musse (Eds.), 15th Brazilian symposium on computer graphics and image processing (pp. 99–105). IEEE Comput. Soc.

Sarver, J. A., Sumey, J. L., Williams, M. L., Bishop, J. P., Dean, D. M., & Kiran, E. (2018). Foaming of poly(ethylene -co- vinyl acetate) and poly(ethylene -co- vinyl acetate -co- carbon monoxide) and their blends with carbon dioxide. Journal of Applied Polymer Science, 135(7), 45841.

Shi, J., Wu, P., Li, L., Liu, T., & Zhao, L. (2009). Crystalline transformation of isotactic polybutene-1 in supercritical CO2 studied by in-situ fourier transform infrared spectroscopy. Polymer, 50(23), 5598–5604.

Swaan Arons, J. de, & Diepen, G. A. M. (1963). Thermodynamic study of melting equilibria under pressure of a supercritical gas. Recueil des Travaux Chimiques des Pays-Bas, 82(3), 249–256.

Takahashi, S., Hassler, J. C., & Kiran, E. (2012). Melting behavior of biodegradable polyesters in carbon dioxide at high pressures. The Journal of Supercritical Fluids, 72, 278–287.

Takebayashi, Y., Sue, K., Furuya, T., Hakuta, Y., & Yoda, S. (2014). Near-infrared spectroscopic solubility measurement for thermodynamic analysis of melting point depressions of biphenyl and naphthalene under high-pressure CO2. The Journal of Supercritical Fluids, 86, 91–99.

van Krevelen, D. W., & Nijenhuis, K. t. (2009). Properties of polymers: Their correlation with chemical structure ; their numerical estimation and prediction from additive group contributions / D.W. van Krevelen (4th, completely rev. ed. / rev. by K. te Nijenhuis). Amsterdam, Boston: Elsevier.

ZAPP, J. A. (1957). Hazards of isocyanates in polyurethane foam plastic production. A.M.A. archives of industrial health, 15(4), 324–330.